CRYSTAL GROWTH & DESIGN

pubs.acs.org/crystal

Article

Complexes of Oligopeptides of Structure-Determining Amino Acids with Phosphotungstic Acid

Björn Greijer, Edgar Stigell, Timothe Guerin, and Vadim G. Kessler*

Cite This: *Cryst. Growth Des.* 2024, 24, 6483−6491

Read Online

ACCESS | Metrics & More | Article Recommendations | Supporting Information

ABSTRACT: Peptides tend to form anisotropic structures, being both asymmetric and chiral. Structure-determining peptides include phenylalanine (Phe) and tyrosine (Tyr) amino acids as they contain aromatic rings, which are sterically demanding and prone to self-assembly via π-stacking. Pursuing the mechanisms of protein interactions with oxide nanoparticles, we used Keggin phosphotungstic acid polyoxometalate (POM) as a model. Six complexes of the POM with different peptide-based ligands were studied, including Phe, Ala (Alanine), and Tyr. Phe−Ala formed a layered structure with pockets of π-stacking involving four Phe residues. Ala−Phe formed two structures based on the rate of formation. The faster forming structure had a loose pattern of POMs in columns surrounded by chains of the ligand with alternating H-bonding and π-stacking. The slower-forming one had a denser network, also with columns of POMs, but with a more complex network of peptides, including π-stacks of three residues appearing as a "web" rather than a "chain". Ala−Ala showed mainly H-bonding connecting the molecules, with the peptide filling the spaces between POMs rather than controlling the structure. Ala seemed to mainly act as a bridge between three POMs, and it had the effect of forming a highly porous structure reminiscent of metal−organic frameworks (MOFs). Tyr formed long columns of the amino acid with both vertical and lateral H-bonding, resulting in alternating layers of POMs and parallel Tyr columns. These structures provide insights into the interactions between biomolecules and POMs, which is valuable for the design and synthesis of POM-derived composite materials.

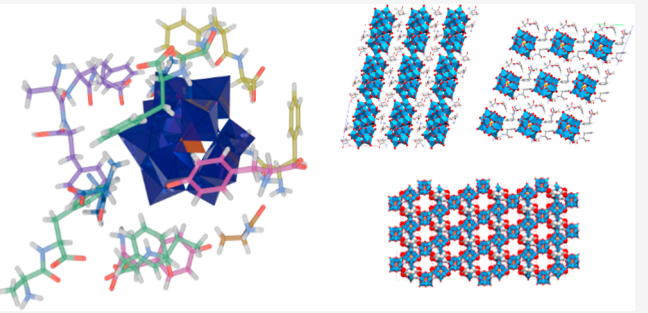

INTRODUCTION

Life has been surrounded by mineral nanoparticles (NPs) since they first emerged in the primordial soup. Weathering of minerals will eventually produce nanomaterials, which remain in bodies of water and affect the organisms living in them.[1] In modern times, such materials are studied and used for a vast number of purposes, are frequently produced artificially, and are occasionally combined with biomolecules to form composite materials.[2]

Self-assembly reactions, such as the sol−gel process,[3] are abundant in nature. Proteins frequently assemble into complex materials, both with a purpose, such as spider silk,[4] and accidentally, such as the amyloid β-peptides plaques which cause Alzheimer's disease.[5] Understanding the mechanism behind these assembly reactions is naturally highly sought after. It has been shown that aromatic residues, tyrosine (Tyr) and phenylalanine (Phe), are often responsible for fiber formation[6,7] and properties.[4]

NPs have been shown to often interact with proteins.[8,9] Determining the nature of the interactions can be difficult in systems as complex as a naturally occurring one; therefore, a model has been developed in order to discover some general principles of the interactions. By using analogues of NPs and proteins, we have developed a model system to study how they might interact.[10−12] This consists of Keggin polyoxometalates (POMs) and oligopeptides. Keggin POMs consist of a central heteroatom within a roughly spherical cage of 12 transition metal atoms in their highest oxidation state, all bridged by oxygen atoms. POMs have frequently been shown to interact with biomolecules.[13−18] In this study, phosphotungstic acid (PW) was used, which has the formula $H_3[PW_{12}O_{40}]$. Oligopeptides are short chains of amino acids, which are the building blocks of proteins. In this study, sequences consisting of alanine (Ala) and phenylalanine (Phe), as well as tyrosine (Tyr), as a single amino acid were used.

Phe and Tyr, as amino acids with an aromatic side chain, play a significant role in controlling the folding of a protein. This is largely due to their ability to form π-bonds with other aromatic groups, providing greater stability to a protein fold or complex. It has been shown that oligopeptides containing

Received: June 12, 2024
Revised: July 17, 2024
Accepted: July 18, 2024
Published: July 26, 2024

https://doi.org/10.1021/acs.cgd.4c00806
Cryst. Growth Des. 2024, 24, 6483−6491

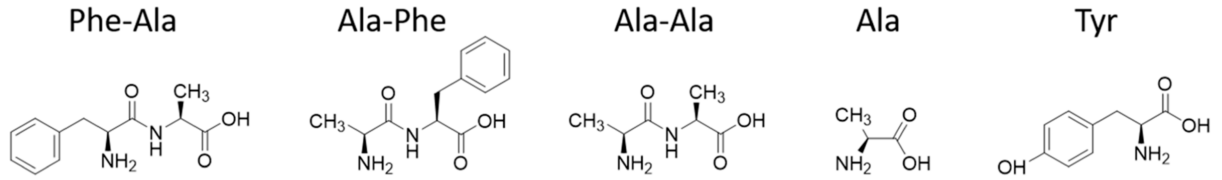

Figure 1. Bonding schemes for ligands applied in this study.

phenylalanine will self-assemble into nanostructures in aqueous media.[6,7] Hybrid materials of POMs and biopolymers are increasingly being developed and used for purposes such as catalysis, adhesion, and biomedicine.[2,19]

Our previous studies on this topic focused mainly on oligoglycines, which demonstrated that POMs can interact with the backbone of proteins in a variety of ways and also how changing the conditions can alter how the same components form crystals.[10−12] Here, we have aimed to investigate how more hydrophobic oligopeptides, such as trialanine, and mixed dipeptides, such as Ala−Phe and Phe−Ala, may interact with NPs.

MATERIALS AND METHODS

All materials were purchased from Sigma-Aldrich and used without further purification. 0.01 mmol of phosphotungstic acid and 0.03 mmol of peptide were dissolved in 5 mL of HCl each (0.1 M for **4** and **6** and 0.5 M for **1**, **2**, **3**, and **5**). The peptide solution was added to the POM solution and mixed in a 15 mL Falcon tube. A portion was transferred to a Petri dish to evaporate quickly. The tube was left open to allow the solvent to evaporate slowly. X-ray quality crystals formed within several months for **1**, **3**, **4**, and **5** in test tubes and within a few days for **2** and **6** in a Petri dish. The ligands used were Phe−Ala for **1**, Ala−Phe for **2** and **3**, Ala−Ala for **4**, Ala−Ala−Ala (degraded to Ala) for **5**, and Tyr for **6**. Single-crystal XRD data was collected using a Bruker D8 QUEST ECO instrument and was processed using the Apex4 software package. Details are given in Supporting Information Methods. EDS was performed with a Hitachi FlexSEM 1000 II instrument (Oxford Instruments) operated by Aztec software. Infrared spectroscopy was performed with a PerkinElmer Spectrum-100 FTIR spectrometer PerkinElmer Spectrum-100.

RESULTS AND DISCUSSION

The peptides used (Figure 1) were chosen for their ability to simulate a more complex part of a protein than our previous studies, which mainly focused on oligoglycines.[10−12] The amino acids used here are both more complex and more hydrophobic, which is more accurate to globular proteins, as they often show a hydrophobic core and a hydrophilic surface. Details of the data collection and refinement are provided in Table 1.

Structure **1** (Figure 2) was found in yellow, block-shaped crystals and forms distinct layers (Figure 2B), with alternating sheets of POMs and peptides. Viewed straight on, the POM layer is arranged in a "mirrored zig zag." The peptides form chains of four π-stacked Phe side chains (Figure 2C) and H-bonds (Figure 2D).

The hydrogen bonding network is extensive, with the shortest bonds being to a particular water molecule and other water molecules and a carbonyl group: O(1)−O(4) 2.495(2) Å, O(1)−O(1Y) 2.535(2) Å, and O(1)−O(6) 2.551(2) Å. Only slightly longer are groups of bonds between peptides and peptides and water: O(2X)−O(10) 2.615(2) Å, O(3X)−O(4) 2.627(2) Å, O(1Y)−O(3Z) 2.662(2) Å, and O(3V)−O(1Z) 2.677(2) Å. Next comes a group of water molecules bonding terminal POM oxygen, amine groups, carboxyl groups, and other water molecules: N(2X)−O(7) 2.698(3) Å, O(35B)−O(8) 2.715(2) Å, O(9)−O(13) 2.741(3) Å, N(2Z)−O(8) 2.752(3) Å, O(1V)−O(9) 2.763(2) Å, O(2)−O(10) 2.781(2) Å, and O(6)−O(9) 2.789(2) Å. A group of bonds with terminal POM oxygen to an amine group, water, and a carboxyl group and terminal POM oxygens and water follows: O(28B)−O(8) 2.792(2) Å, O(38B)−N(2X) 2.794(1) Å, O(34B)−O(10) 2.822(1) Å, O(26A)−O(4) 2.825(2) Å, and O(25A)−O(27B) 2.838(1) Å. Next is a mixed group of bonds with terminal and bridging POM oxygen, water, amine groups, and carboxyl groups, with most combinations represented: N(2V)−O(2Z) 2.842(2) Å, O(13B)−O(6) 2.845(1) Å, O(24A)−N(2X) 2.847(2) Å, O(3)−O(2) 2.847(2) Å, O-(31B)−N(2X) 2.855(2) Å, N(2Y)−O(9) 2.890(1) Å, O-(30A)−O(12) 2.900(1) Å, O(29B)−O(2V) 2.902(3) Å, O(37A)−O(31B) 2.903(3) Å, O(2Y)−O(13) 2.914(2) Å, O(9B)−O(5) 2.926) Å, O(10)−O(11) 2.931(4) Å, N(2V)−O(12) 2.933(3) Å, N(2Z)−O(5) 2.942(1) Å, and O(2Y)−N(2Z) 2.946(1) Å. Next comes a series of bonds with mostly POM oxygens or water molecules bonding amine, amide, carbonyl groups, water molecules, and each other: O(28A)−O(33B) 2.947(2) Å, O(25A)−O(28B) 2.947(2) Å, O(30B)−O(4) 2.961(2) Å, O(39B)−N(2V) 2.963(4) Å, O(1X)−O(11) 2.965(1) Å, O(11A) N(1Y) 2.966(2) Å, O(33B)−O(12) 2.966(2) Å, O(36B)−O(3Y) 2.969(3) Å, N(2Z)−O(6) 2.972(1) Å, O(5)−O(7) 2.977(2) Å, N(2Y)−O(2) 2.978(3) Å, O(30A)−O(34B) 2.980(1) Å, O(33A)−N(2V) 2.992(2) Å, and O(18B)−O(2) 2.993(2) Å. Pushing the upper limit of hydrogen bonding, but still worth noting, are a group of bonds between carbonyl, carboxyl, and amide groups and water or POM oxygen, as well as POM−POM contacts: O(2Y)−O(1) 3.003(1) Å, O(33A)−O(34B) 3.028(1) Å, O(12A)−O(5) 3.028(1) Å, O(36B)−O(3X) 3.030(2) Å, O(39A)−O(29B) 3.032(2) Å, O(2Y)−O(6) 3.038(2) Å, and O(39A)−N(1X) 3.060(2) Å.

Some of the bonds to O1 are extremely short, but this can be attributed to the tight packing and strong attractive forces between the molecules. The oxygen atoms O1−O13 do not have hydrogen placed on them, but it is clear from their placement and bonding patterns that they are, in fact, water molecules. O9 and O10 appear to have bond angles close to those of oxonium ions and are likely protonated. The close contacts between POMs are likely due to protonation of the POM, as they are in the range of H-bonds.

In contrast to **1**, the needle-shaped crystals of **2** (Figure 3) do not form layers, but rather columns of POMs surrounded by a matrix of peptides (Figure 3B). The peptides form chains of alternating H-bonds between peptides, POMs and water molecules (Figure 3C), and π-stacked Phe side chains (Figure 3D).

The shortest contacts are between carboxyl groups and an amino group N(1B)−O(2A) 2.658(8) Å or water O(1B)−O(1X) 2.838(6) Å. Slightly longer are bonds terminal POM oxygen and an amide group O(18)−N(2B) 2.903(4) Å, a

https://doi.org/10.1021/acs.cgd.4c00806
Cryst. Growth Des. 2024, 24, 6483−6491

Table 1. Crystallographic Data for Compounds 1−6

			1	2	3	4	5	6
chemical formula			$C_{36}H_{48}N_6O_{49}PW_{12}$	$C_{24}H_{43}N_4O_{50}PW_{12}$	$C_{18}H_{23}N_3O_{24.5}P_{0.5}W_6$	$C_{12}H_{21}N_4O_{50}PW_{12}$	$C_6H_{19}N_2O_{71}P_{1.5}W_{18}$	$C_{18}H_{24}SN_2O_{48}PW_{12}$
formula weight			3445.20 g/mol	3423.78 g/mol	1791.98 g/mol	3257.49 g/mol	4605.95 g/mol	3273.56 g/mol
temperature			293(2) K	293(2) K	293(2) K	293(2) K	293(2) K	295(2) K
wavelength			0.71073 Å	0.71073 Å	0.71076 Å	0.71073 Å	0.71073 Å	0.71073 Å
crystal size			0.130 × 0.180 × 0.240 mm	0.020 × 0.080 × 0.210 mm	0.300 × 0.300 × 0.800 mm	0.010 × 0.080 × 0.100 mm	0.320 × 0.340 × 0.540 mm	0.020 × 0.020 × 0.100 mm
crystal system			monoclinic	monoclinic	triclinic	monoclinic	orthorhombic	triclinic
space group			$P12_11$	$P12_11$	$P\bar{1}$	$P12_11$	$C222$	$P\bar{1}$
unit cell dimensions	a	α	15.0118(6) Å 90°	9.737(6) Å 90°	9.8759(8) Å 65.914(3)°	9.9033(5) Å 90°	16.1458(8) Å 90°	14.516(4) Å 79.727(6)°
	b	β	26.6598(12) Å 101.782(2)°	26.169(16) Å 103.931(11)°	14.3510(11) Å 76.635(4)°	26.5990(14) Å 90.8930(10)°	34.5595(17) Å 90°	14.786(5) Å 75.244(7)°
	c	γ	15.5858(6) Å 90°	14.337(9) Å 90°	14.6921(11) Å 75.416(3)°	10.0515(5) Å 90°	12.9893(6) Å 90°	15.519(5) Å 65.402(6)°
volume			6106.2(4) Å^3	3546.(4) Å^3	1820.2(3) Å^3	2647.4(2) Å^3	7247.9(6) Å^3	2918.8(15) Å^3
Z			4	2	2	2	4	2
theta range for data collection			2.06 to 35.26°	2.14 to 28.13°	2.44 to 34.98°	2.17 to 35.13°	2.52 to 35.11°	2.12 to 26.60°
index ranges			$-24 \le h \le 24$	$-12 \le h \le 12$	$-15 \le h \le 15$	$-16 \le h \le 15$	$-25 \le h \le 23$	$-18 \le h \le 18$
			$-42 \le k \le 42$	$-34 \le k \le 34$	$-21 \le k \le 22$	$-42 \le k \le 42$	$-55 \le k \le 55$	$-18 \le k \le 18$
			$-24 \le l \le 24$	$-18 \le l \le 18$	$-23 \le l \le 23$	$-15 \le l \le 16$	$-20 \le l \le 20$	$-19 \le l \le 19$
reflections collected			103,478	49,681	24,187	49,121	48,469	26,319
independent reflections			50,215 [R(int) = 0.0500]	17,101 [R(int) = 0.0490]	19,537 [R(int) = 0.0342]	21,811 [R(int) = 0.0561]	15,371 [R(int) = 0.0999]	11,856 [R(int) = 0.0769]
no. of observed independent reflections; $I > 2\sigma(I)$			42,803	13,023	13,164	15,898	12,863	7309
final R indices, observed			$R1$ = 0.0402, w$R2$ = 0.0867	$R1$ = 0.0497, w$R2$ = 0.1172	$R1$ = 0.0617, w$R2$ = 0.1364	$R1$ = 0.0548, w$R2$ = 0.1276	$R1$ = 0.0463, w$R2$ = 0.1073	$R1$ = 0.0708, w$R2$ = 0.1789
final R indices, all data			$R1$ = 0.0527, w$R2$ = 0.0915	$R1$ = 0.0751, w$R2$ = 0.1289	$R1$ = 0.1062, w$R2$ = 0.1564	$R1$ = 0.0830, w$R2$ = 0.1469	$R1$ = 0.0603, w$R2$ = 0.1131	$R1$ = 0.1233, w$R2$ = 0.2049

https://doi.org/10.1021/acs.cgd.4c00806
Cryst. Growth Des. 2024, 24, 6483−6491

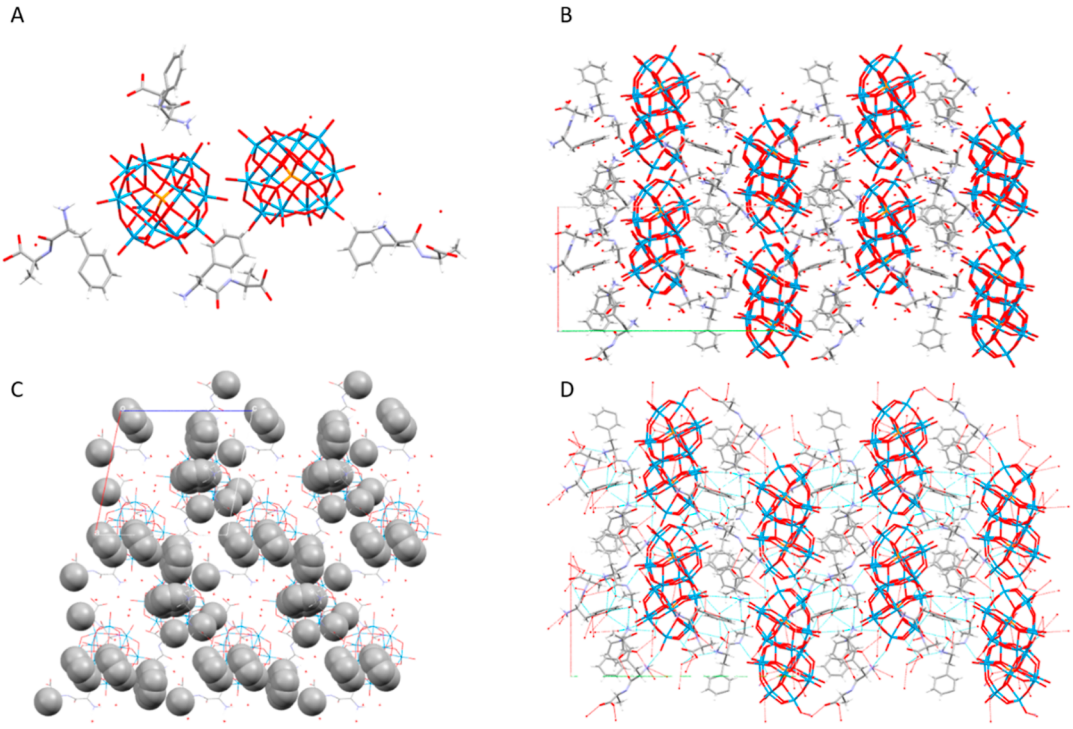

Figure 2. Structure **1** $[(H_3O)_2(HPhe\text{-}Ala)_4[PW_{12}O_{40}]_2 \cdot 11H_2O]$ shown as (A) molecular arrangement and (B) packing. Highlighted are (C) hydrophobic groups and (D) H-bonds.

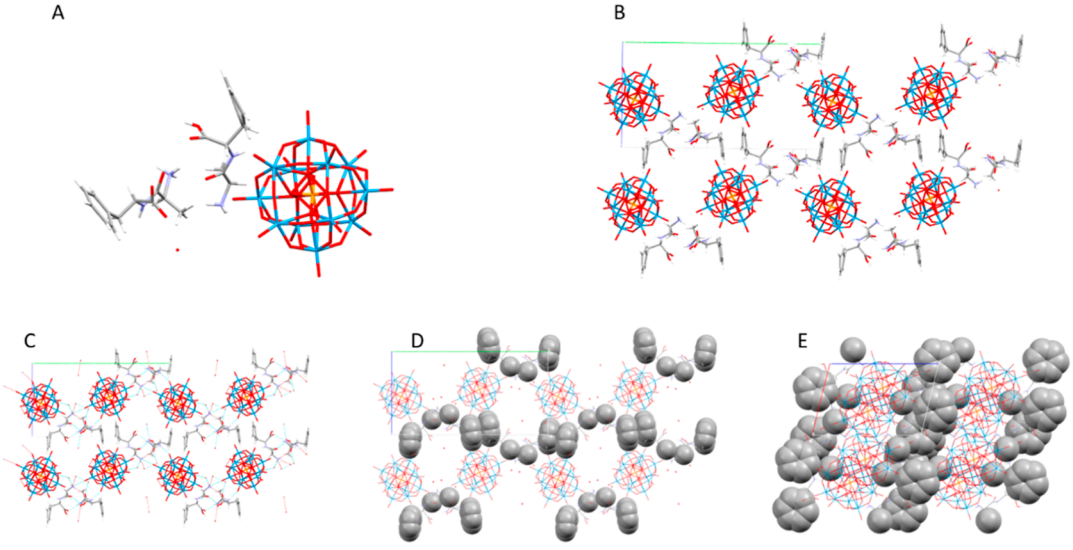

Figure 3. Structure **2** $[(HAla\text{-}Phe)_2[HPW_{12}O_{40}] \cdot 4H_2O]$ shown as (A) molecular arrangement and (B) crystal packing. Highlighted are (C) H-bonding and hydrophobic interactions viewed from the side (D) and from the top (E).

bridging POM oxygen O(16)−O(15) 2.906(4) Å, an amino group O(42)−N(1A) 2.938(4) Å, as well as a contact between an amino group and a carbonyl group N(1B)−O(3A) 2.909(7) Å. Next are a contact between a terminal and bridging POM oxygen O(25)−O(40) 2.961(3) Å, a carboxyl group and an amino group O(1B)−N(1A) 2.973(5) Å, and several contacts between terminal POM oxygen O(16)−O(41) 2.977(3) Å, O(38)−O(11) 3.007(3) Å, and O(18)−O(40) 3.037(3) Å. In addition, there is π-stacking between the Phe side chains. These form pairs from nonequivalent peptides and lie in a parallel displaced conformation (Figure 3E).

Despite containing the same components as **2**, the structure of **3** (Figure 4) is quite different. First, the crystal was block-like. Second, the structure appears to be more dense, containing no water molecules and showing less porosity. The POMs are arranged in columns, surrounded by a matrix of peptides, but the peptides are arranged less like a chain and more like a net, with connections to each other in three dimensions (Figure 4B). These connections are both π-stacking (Figure 4C) and H-bonding (Figure 4D), with the former in both face−face and face−edge conformations.

The shortest H-bonds are between carbonyl groups and a carboxyl group O(3B)−O(1C) 2.612(4) Å, and two amino

https://doi.org/10.1021/acs.cgd.4c00806
Cryst. Growth Des. 2024, 24, 6483−6491

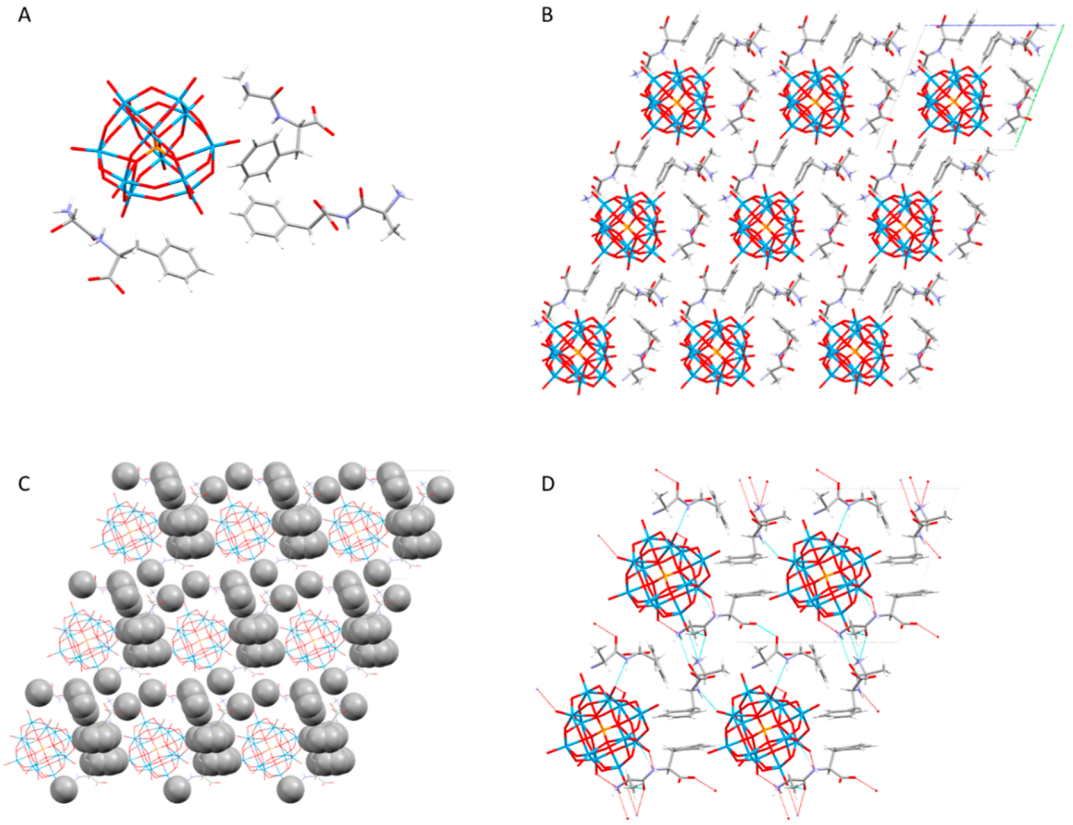

Figure 4. Structure **3** $[(HAla\text{-}Phe)_3[PW_{12}O_{40}]]$ shown as (A) molecular arrangement and (B) crystal packing. Highlighted are (C) hydrophobic groups and (D) H-bonding.

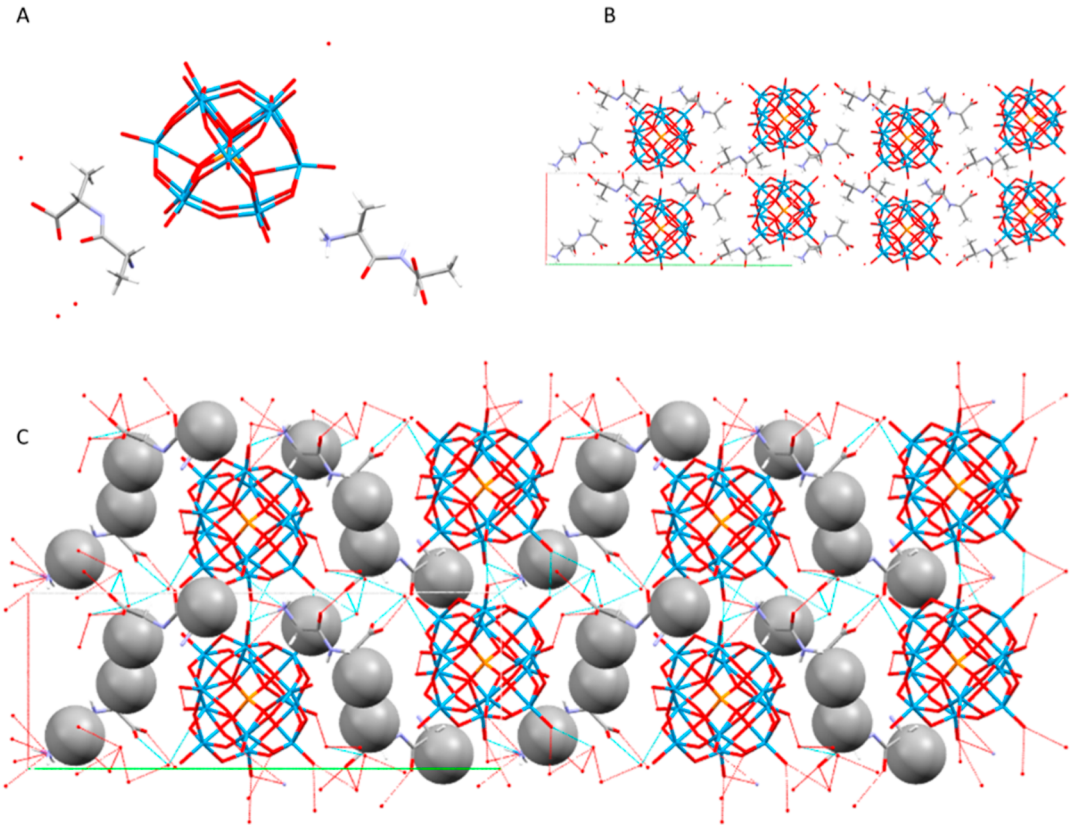

Figure 5. Structure **4** $[(HAla\text{-}Ala)_2[HPW_{12}O_{40}]\cdot 4H_2O]$ shown as (A) molecular arrangement and (B) crystal packing. Highlighted are (C) H-bonding and hydrophobic interactions.

https://doi.org/10.1021/acs.cgd.4c00806
Cryst. Growth Des. 2024, 24, 6483−6491

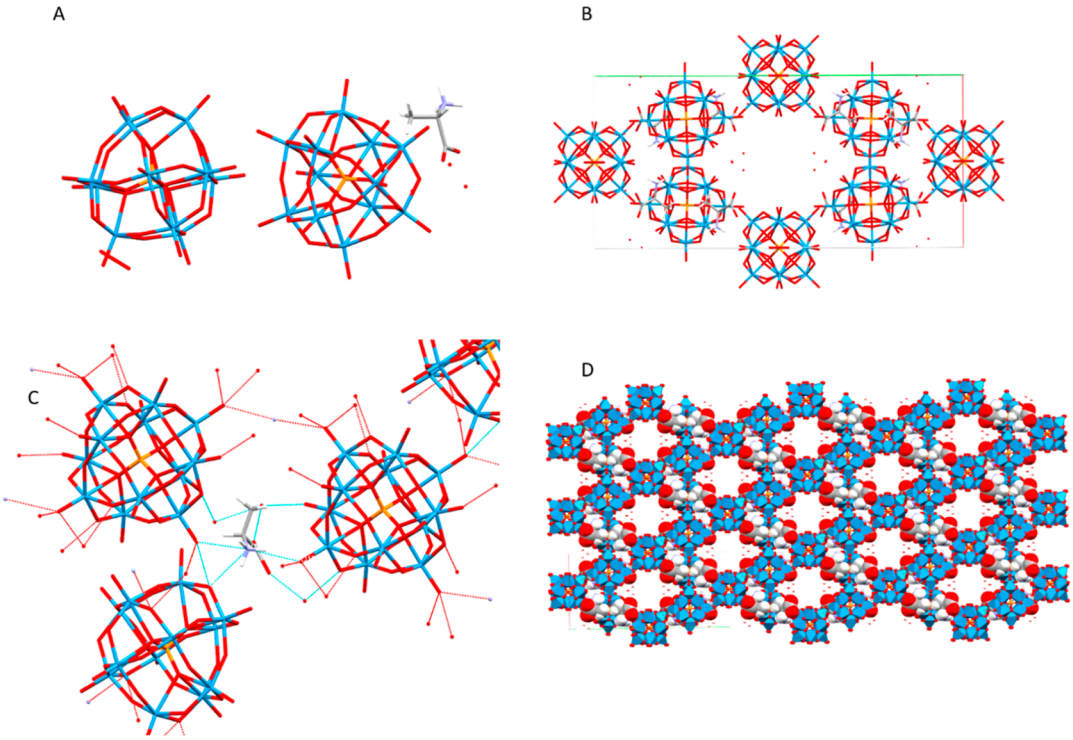

Figure 6. Structure **5** $[(HAla)H_5[PW_{12}O_{40}]_2{\cdot}4H_2O]$ shown as (A) molecular arrangement and (B) crystal packing. Highlighted are (C) H-bonding and the (D) MOF-like matrix.

groups O(1B)−N(1A) 2.797(3) Å, N(1B)−O(1A) 2.841(3) Å. The rest of the H-bonds are to terminal POM oxygen, with other terminal POM oxygens O(25)−O(1) 2.868(3), O(12)−O(9) 3.017), bridging POM oxygen O(18)−O(9) 2.895(2) Å, amine groups O(27)−N(1B) 2.906(4) Å, O(37)−N(1A) 2.948(3) Å, amide groups O(1)−N(2C) 2.992(3) Å, O(36)−N(2A) 2.996(3) Å, O(9)−N(2B) 3.001(3) Å, O(12)−N(2B) 3.018(3) Å, and a carbonyl group O(37)−O(1B) 3.023(3) Å.

The colorless, block-shaped crystals forming the structure of **4** (Figure 5) contain far more H-bonds compared to complexes **2** and **3**, likely due to the comparatively lower hydrophobicity of the peptide. The main force directing this structure appears to be H-bonding, while in **2** and **3**, it appears to be π-stacking, though van der Waals interactions (approximately 4 Å) between the Ala side chains are visible (Figure 5C).

The shortest H-bonds are between carboxyl groups and carbonyl groups, O(3A)−O(2B) 2.655(4) Å and O(2A)−O(3B) 2.666(3) Å, and between water molecules, O(1X)−O(2X) 2.669(9) Å, O(2X)−O(4X) 2.727(10), and O(2X)−O(3X) 2.779(10) Å. Next are contacts between water molecules and carboxyl groups, O(1B)−O(1X) 2.718(4) Å, O(1A)−O(3X) 2.871(6) Å, terminal POM oxygen O(30)−O(4X) 2.862(4) Å, O(32)−O(3X) 2.917(5) Å, or bridging POM oxygen O(9)−O(1X) 2.932(3) Å. The longest H-bonds are between two terminal POM oxygens, O(30)−O(38) 2.960(3) Å, O(4)−O(6) 2.977(2) Å, and O(34)−O(39) 3.038(3) Å, a carboxyl group and a water molecule, O(2A)−O(4X) 3.003(5) Å, terminal POM oxygen, and one particular amino group, O(31)−N(2B) 2.962(3) Å, and O(4)−N(2B) 2.988(3) Å, and O(6)−N(2B) 3.017(3) Å and O(37)−N(2B) 3.029(3) Å, a water molecule, O(38)−O(4X) 2.963(4) Å, or bridging POM oxygen, O(7)−O(31) 3.018(3) Å and O(37)−O(12) 3.023(3) Å. In addition, two Ala side chains form a van der Waals interaction, with C(3A)−C(3B) 4.023(8) Å.

Structure **5** (Figure 6) was synthesized using trialanine, though it contains only the monomer, and formed large, colorless, block-shaped crystals. Most likely, the acidic conditions degraded the peptide bonds over time, as the sample was left for several months before crystals formed. The structure is remarkably porous, with voids approximately 12 × 8 × 5 Å in volume (Figure 6B,D). This structure is reminiscent of metal−organic frameworks (MOFs), though as it is held together by H-bonds (Figure 6C) rather than covalent bonds, it should not be considered a true MOF.

The H-bonding network is extensive, with the shortest contacts being between water and a carboxyl group, O(2A)−O(3AA) (2.454(7) Å), and two water molecules, O(1AA)−O(4AA) 2.637(6) Å. Slightly longer are H-bonds between bridging POM oxygen and water O(22)−O(3AA) 2.782(5) Å, terminal POM oxygen and the amine group O(25)−N(1A) 2.788(2) Å, O(17)−N(1A) 2.910(2) Å, and terminal POM oxygen and water O(18)−O(4AA) 2.923(5) Å. The longest contacts are between POM oxygens O(24)−O(17) 2.929(2) O(25)−O(7) 2.960(1) Å, O(17)−O(17) 2.973(2) Å, and O(25)−O(25) 3.028(2) Å, bridging POM oxygen and the amine group O(7)−N(1A) 2.959(2) Å, a carboxyl group and water O(1A)−O(1AA) 3.008(5) Å, and terminal POM oxygen and water O(11)−O(1AA) 3.028(3) Å. In addition, there are hydrophobic interactions between the Ala side chains, causing the formation of isolated pairs of the amino acid between the POMs. The amine group is in contact with three adjacent POMs (Figure 5C), and each such triad is touched by two amine groups at the center. The pattern of the side chains interacting with each other is reflected in the structure of pure L-alanine,[20] as well as in those of leucine[21] and isoleucine,[22] begging the question of whether a MOF-like structure with

https://doi.org/10.1021/acs.cgd.4c00806
Cryst. Growth Des. 2024, 24, 6483−6491

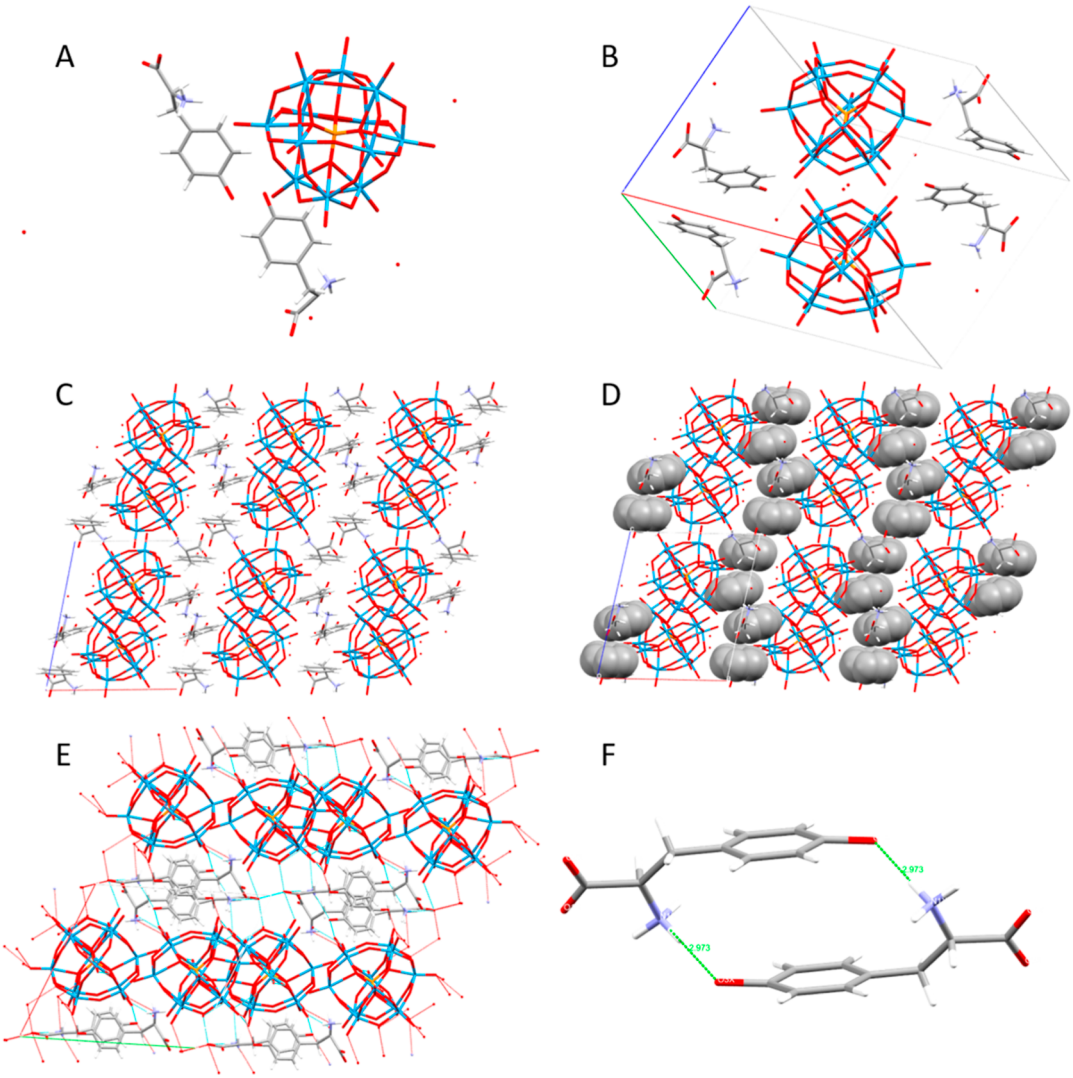

Figure 7. Structure **6** $[(HTyr)_2[HPW_{12}O_{40}]\cdot 4H_2O]$ shown as (A) molecular arrangement and (B) crystal packing. Highlighted are the (C) layering of the packing, (D) chains of π-stacked rings, (E) H-bonding in the whole structure, and (F) H-bonding between stacked amino acids.

larger voids could be produced using the amino acids with longer side chains.

6 (Figure 7) is a light brown, needle-shaped crystal, with phosphotungstate forming a complex with an amino acid rather than an oligopeptide, though its relevance for the sake of comparison with Phe cannot be overlooked. Tyr has a carbonyl group on the phenyl ring, allowing for additional H-bonding as well as π-stacking. The structure shows a chain of stacked rings (Figure 7C,D), with the amino acids alternating in the direction, allowing for lateral connections between stacks (Figure 7E), as well as occasional H-bonds between the carbonyl and amine groups (Figure 7F).

The structure contains a number of H-bonds, the shortest of which are between water and a carboxyl group O(1X)−O(2A) 2.719(4) Å, two water molecules O(2A)−O(3A) 2.767(5) Å, and between terminal POM oxygen and carbonyl groups O(33)−O(3X) 2.793(3) Å, O(29)−O(3Y) 2.804(3) Å. Slightly weaker are bonds between water molecules and terminal POM oxygen O(21)−O(6A) 2.869(6) Å; an amine group, N(1X)−O(2A) 2.894(4) Å; bridging POM oxygen O(7)−O(4A) 2.897(4) Å; and terminal POM oxygen O(5)−O(6A) 2.897(6) Å. Next come bonds between terminal POM oxygens O(29)−O(49) 2.904(3) Å, O(34)−O(39) 2.957(3) Å, bridging POM oxygen and water O(24)−O(3A) 2.914(6) Å, terminal POM oxygen and an amine group O(34)−N1X) 2.944(3) Å, and a carbonyl group and an amine group O(3X)−N(1X) 2.973(3) Å. The weakest bonds are from terminal POM oxygen to other terminal POM oxygens, O(5)−O(21) 2.980(2) Å, O(18)−O(21) 2.988(3) Å, an amine group, O(36)−N(1Y) 2.984(3), bridging POM oxygen, O(26)−O(34) 2.991(4) Å, and water, O(38)−O(2A) 3.024(3) Å. In addition to H-bonds, there are π-interactions between the aromatic rings in the side chains.

It should be noted that atoms C(2Y), C(3Y), O(1Y), and N(1Y) are highly disordered, and their positions may in reality be more varied than the structure suggests, and atom C(2X) was disordered and had to be treated to fix thermal deviation parameter for the most probably atomic arrangement. There are also voids likely containing a disordered solvent.

EDS spectra of **1**, **3**−**6** were taken (Figure S1), showing the composition to be of tungsten, phosphorus, oxygen, nitrogen, and carbon in the approximate ratios one would expect from the structure (Tables S1−S5), with minor variations likely due to dried mother liquor, which also explains the presence of

https://doi.org/10.1021/acs.cgd.4c00806
Cryst. Growth Des. 2024, 24, 6483−6491

chloride in some samples. FTIR spectra of **1**, **3**−**5** were taken (Figure S2−S5), showing that the carboxyl groups are likely protonated for those peptides.

The Phe-containing structures all displayed isolated pockets of π-stacking, while H-bonding to the environment occurred via the oxygen- and nitrogen-containing groups. The same pattern is found in globular proteins, which typically have a hydrophobic core and a hydrophilic surface. Ala-containing peptides had a weak tendency to place the Ala side chains in contact with each other, likely due to their hydrophobicity. We have shown previously that longer oligopeptides tend to direct structure formation more strongly than shorter ones, and may cause a different ratio of POM to peptide in the crystal than there was in solution,[10,11] as was also the case here. It is reasonable to suggest that the side chains direct complex formation before crystal nucleation and so dictate the structure of the crystal to a degree. This is much like how a protein will fold its hydrophobic side chains toward each other as it is extruded from the ribosome, while hydrophilic groups seek each other to form the secondary structures of α-helices and β-sheets.

As for the contacts between peptides and POMs, **1** shows mainly H-bonding with the amine group, and **2** has only two direct contacts, with amine and amide groups. **3** also has both types, but more of them. **4** has several H-bonds to amine groups, and **5** has two amine groups central to each POM triad. In **6**, POMs have H-bonds to the amino group, as well as the carbonyl group on the ring. The rings in **1**−**3** lie with the edge toward POMs, while in **6**, the angle is less perpendicular but still not face-on. All rings appear wedged between terminal oxygen and lie closer to the bridging oxygen.

The difference between compounds **2** and **3** is notable. **3** appears more dense, with no water or cavities in the structure. The main difference between their syntheses is the speed of formation. A slower evaporation yielded a denser and more highly ordered packing, in that **2** showed "chains" of peptides (Figure 3B), while **3** showed a "web" of peptides (Figure 4B). **3** also has three rings involved in their stacks, compared to the pairs in **2**. The additional time afforded to **3** may have allowed for a more sophisticated network, possibly by allowing the peptides to arrange themselves into stable clusters before the nucleation event, although the exact dynamics remain to be determined. As phosphotungstate is considered a super-chaotropic ion,[23] it may be that chaotropic forces affect **2** more strongly than **3**. **2** and **3** should also be compared to **1**. Simply switching the order of the amino acids produced a remarkably different structure. Not only does **1** display nearly twice the H-bonds compared to **2** and **3** (normalized against Z), but the POMs are also arranged in layers rather than the columns seen in **2** and **3**. Again, a seemingly insignificant factor produced a major effect on the structure. Finally, **6** should be compared to **1**, **2**, and **3**. As with Phe, it is clear that π-interactions from Tyr molecules are the main force forming the structure. Adding the possibility of H-bonding to the carbonyl group and the lack of steric hindrance from other residues, the stacks form long chains rather than isolated pockets, somewhat inverting the pattern of POM columns in **2** and **3**. The stacks and POMs are also arranged in layers, reflecting the motif in **1**. Tyr-forming H-bonds support the findings that they are partially responsible for deformation of spider silk fibers in high humidity.[4] The findings presented here also imply that NPs have the capacity to impact the structure and properties of protein-based composite materials. The MOF-like **5** may also deserve some interest, as polyoxometalate-based MOFs (PMOFs) have gained attention in recent years.[24] Li and Wu[25] outline how amphiphilic ligands can form supramolecular frameworks by binding a POM at the hydrophilic head and one another at the hydrophobic tail, which is exactly what can be seen in structure **5**. Using POMs and amino acids, instead of late transition metals and polypyridines or carboxylates, as materials for H-bonded nanoporous structures could present a distinct advantage.

CONCLUSIONS

Six structures of complexes with Phe, Ala, or Tyr with phosphotungstic acid have been synthesized. Columns of NPs surrounded by an organic framework and columns of π-stacked aromatic rings could be expected in composite materials with similar precursors. The addition of hydrophobic peptides moves structures from standard hexagonal packing seen for spherical particles such as Keggin POMs, and instead, we see cubic packing for many of these structures enforced by the self-assembly of the peptide ligands. These structures reveal core principles behind the formation of NP-biomolecule composites and may be used for a more refined method of designing such materials.

ASSOCIATED CONTENT

Supporting Information

The Supporting Information is available free of charge at https://pubs.acs.org/doi/10.1021/acs.cgd.4c00806.

Details of data collection and refinement for all six structures, EDS analysis of crystals of all obtained materials (both spectra and contents of elements in table form), FTIR spectra of compounds **3**−**5** with indication of most important adsorption bands, and atomic coordinates and selected bond lengths and angles for compounds **1**−**6** (PDF)

Accession Codes

CCDC 2362067−2362072 contain the supplementary crystallographic data for this paper. These data can be obtained free of charge via www.ccdc.cam.ac.uk/data_request/cif, or by emailing data_request@ccdc.cam.ac.uk, or by contacting The Cambridge Crystallographic Data Centre, 12 Union Road, Cambridge CB2 1EZ, UK; fax: +44 1223 336033.

AUTHOR INFORMATION

Corresponding Author

Vadim G. Kessler − *Department of Molecular Sciences, Swedish University of Agricultural Sciences, Uppsala 750 07, Sweden*; orcid.org/0000-0001-7570-2814; Email: vadim.kessler@kemi.slu.se

Authors

Björn Greijer − *Department of Molecular Sciences, Swedish University of Agricultural Sciences, Uppsala 750 07, Sweden*

Edgar Stigell − *Department of Molecular Sciences, Swedish University of Agricultural Sciences, Uppsala 750 07, Sweden*

Timothe Guerin − *Department of Molecular Sciences, Swedish University of Agricultural Sciences, Uppsala 750 07, Sweden*

Complete contact information is available at: https://pubs.acs.org/10.1021/acs.cgd.4c00806

Notes

The authors declare no competing financial interest.

https://doi.org/10.1021/acs.cgd.4c00806
Cryst. Growth Des. 2024, 24, 6483−6491

■ ACKNOWLEDGMENTS

The authors are grateful to Prof. Gulaim Seisenbaeva for valuable comments and help with FTIR measurements. The support from the Swedish Research Council (Vetenskapsrådet) to the grant Molecular mechanisms in oxide nanoparticle interactions with proteins, 2022-03971_VR, is gratefully acknowledged.

■ REFERENCES

(1) Sharma, V. K.; Filip, J.; Zboril, R.; Varma, R. S. Natural Inorganic Nanoparticles − Formation, Fate, and Toxicity in the Environment. *Chem. Soc. Rev.* **2015**, *44* (23), 8410−8423.
(2) Soria-Carrera, H.; Atrián-Blasco, E.; Martín-Rapún, R.; Mitchell, S. G. Polyoxometalate−Peptide Hybrid Materials: From Structure−Property Relationships to Applications. *Chem. Sci.* **2023**, *14* (1), 10−28.
(3) Kessler, V. G.; Seisenbaeva, G. A. Molecular Mechanisms of the Metal Oxide Sol-Gel Process and Their Application in Approaches to Thermodynamically Challenging Complex Oxide Materials. *J. Sol-Gel Sci. Technol.* **2023**, *107* (1), 190−200.
(4) Greco, G.; Arndt, T.; Schmuck, B.; Francis, J.; Bäcklund, F. G.; Shilkova, O.; Barth, A.; Gonska, N.; Seisenbaeva, G.; Kessler, V.; Johansson, J.; Pugno, N. M.; Rising, A. Tyrosine Residues Mediate Supercontraction in Biomimetic Spider Silk. *Commun. Mater.* **2021**, *2* (1), 43.
(5) Hardy, J.; Selkoe, D. J. The Amyloid Hypothesis of Alzheimer's Disease: Progress and Problems on the Road to Therapeutics. *Science* **2002**, *297* (5580), 353−356.
(6) Kurbasic, M.; Garcia, A. M.; Viada, S.; Marchesan, S. Tripeptide Self-Assembly into Bioactive Hydrogels: Effects of Terminus Modification on Biocatalysis. *Molecules* **2021**, *26* (1), 173.
(7) Marchesan, S.; Vargiu, A. V.; Styan, K. E. The Phe-Phe Motif for Peptide Self-Assembly in Nanomedicine. *Molecules* **2015**, *20* (11), 19775−19788.
(8) Lynch, I.; Dawson, K. A. Protein-Nanoparticle Interactions. *Nano Today* **2008**, *3* (1−2), 40−47.
(9) Cedervall, T.; Lynch, I.; Lindman, S.; Berggard, T.; Thulin, E.; Nilsson, H.; Dawson, K. A.; Linse, S. Understanding the Nanoparticle-Protein Corona Using Methods to Quantify Exchange Rates and Affinities of Proteins for Nanoparticles. *Proc. Natl. Acad. Sci. U.S.A.* **2007**, *104* (7), 2050−2055.
(10) Rominger, K. M.; Nestor, G.; Eriksson, J. E.; Seisenbaeva, G. A.; Kessler, V. G. Complexes of Keggin POMs [PM12O40]3− (M = Mo, W) with GlyGly Peptide and Arginine—Crystal Structures and Solution Reactivity. *Eur. J. Inorg. Chem.* **2019**, *2019* (39−40), 4297−4305.
(11) Greijer, B.; De Donder, T.; Nestor, G.; Eriksson, J. E.; Seisenbaeva, G. A.; Kessler, V. G. Complexes of Keggin POMs [PM12O40]3− (M = Mo, W) with GlyGlyGly and GlyGlyGlyGly Oligopeptides. *Eur. J. Inorg. Chem.* **2021**, *2021* (1), 54−61.
(12) Greijer, B. H.; Nestor, G.; Eriksson, J. E.; Seisenbaeva, G. A.; Kessler, V. G. Factors Influencing Stoichiometry and Stability of Polyoxometalate − Peptide Complexes. *Dalton Trans.* **2022**, *51* (24), 9511−9521.
(13) Absillis, G.; Parac-Vogt, T. N. Peptide Bond Hydrolysis Catalyzed by the Wells−Dawson $Zr(\alpha_2\text{-}P_2W_{17}O_{61})_2$ Polyoxometalate. *Inorg. Chem.* **2012**, *51* (18), 9902−9910.
(14) Vandebroek, L.; Van Meervelt, L.; Parac-Vogt, T. N. Direct Observation of the ZrIV Interaction with the Carboxamide Bond in a Noncovalent Complex between Hen Egg White Lysozyme and a Zr-Substituted Keggin Polyoxometalate. *Acta Crystallogr., Sect. C: Struct. Chem.* **2018**, *74* (11), 1348−1354.
(15) Ly, H. G. T.; Parac-Vogt, T. N. Spectroscopic Study of the Interaction between Horse Heart Myoglobin and Zirconium(IV)-Substituted Polyoxometalates as Artificial Proteases. *ChemPhysChem* **2017**, *18* (18), 2451−2458.
(16) Bijelic, A.; Aureliano, M.; Rompel, A. The Antibacterial Activity of Polyoxometalates: Structures, Antibiotic Effects and Future Perspectives. *Chem. Commun.* **2018**, *54* (10), 1153−1169.
(17) Breibeck, J.; Bijelic, A.; Rompel, A. Transition Metal-Substituted Keggin Polyoxotungstates Enabling Covalent Attachment to Proteinase K upon Co-Crystallization. *Chem. Commun.* **2019**, *55* (77), 11519−11522.
(18) Bijelic, A.; Dobrov, A.; Roller, A.; Rompel, A. Binding of a Fatty Acid-Functionalized Anderson-Type Polyoxometalate to Human Serum Albumin. *Inorg. Chem.* **2020**, *59* (8), 5243−5246.
(19) Zhao, Y.; Wang, Z.; Ni, J.; He, P. Self-Assembly of Polyoxometalate Clusters into Nanostructures with Different Dimensions. *Eur. J. Inorg. Chem.* **2024**, No. e202400184.
(20) Simpson, H. J.; Marsh, R. E. The Crystal Structure of L-Alanine. *Acta Crystallogr.* **1966**, *20* (4), 550−555.
(21) Coll, M.; Solans, X.; Font-Altaba, M.; Subirana, J. A. Structure of L-Leucine: A Redetermination. *Acta Crystallogr., Sect. C: Struct. Chem.* **1986**, *42* (5), 599−601.
(22) Torii, K.; Iitaka, Y. The Crystal Structure of L-Isoleucine. *Acta Crystallogr., Sect. B: Struct. Sci., Cryst. Eng. Mater.* **1971**, *27* (11), 2237−2246.
(23) Assaf, K. I.; Nau, W. M. The Chaotropic Effect as an Assembly Motif in Chemistry. *Angew. Chem., Int. Ed.* **2018**, *57* (43), 13968−13981.
(24) Zhang, Y.; Liu, Y.; Wang, D.; Liu, J.; Zhao, J.; Chen, L. State-of-the-Art Advances in the Syntheses, Structures, and Applications of Polyoxometalate-Based Metal−Organic Frameworks. *Polyoxometalates* **2023**, *2* (1), 9140017.
(25) Li, B.; Wu, L. Perspective of Polyoxometalate Complexes on Flexible Assembly and Integrated Potentials. *Polyoxometalates* **2023**, *2* (1), 9140016.

https://doi.org/10.1021/acs.cgd.4c00806
Cryst. Growth Des. 2024, 24, 6483−6491